Voltage-Gated Ca^{2+} Channels

Please press the "Back" button to return to the previous menu

BACK

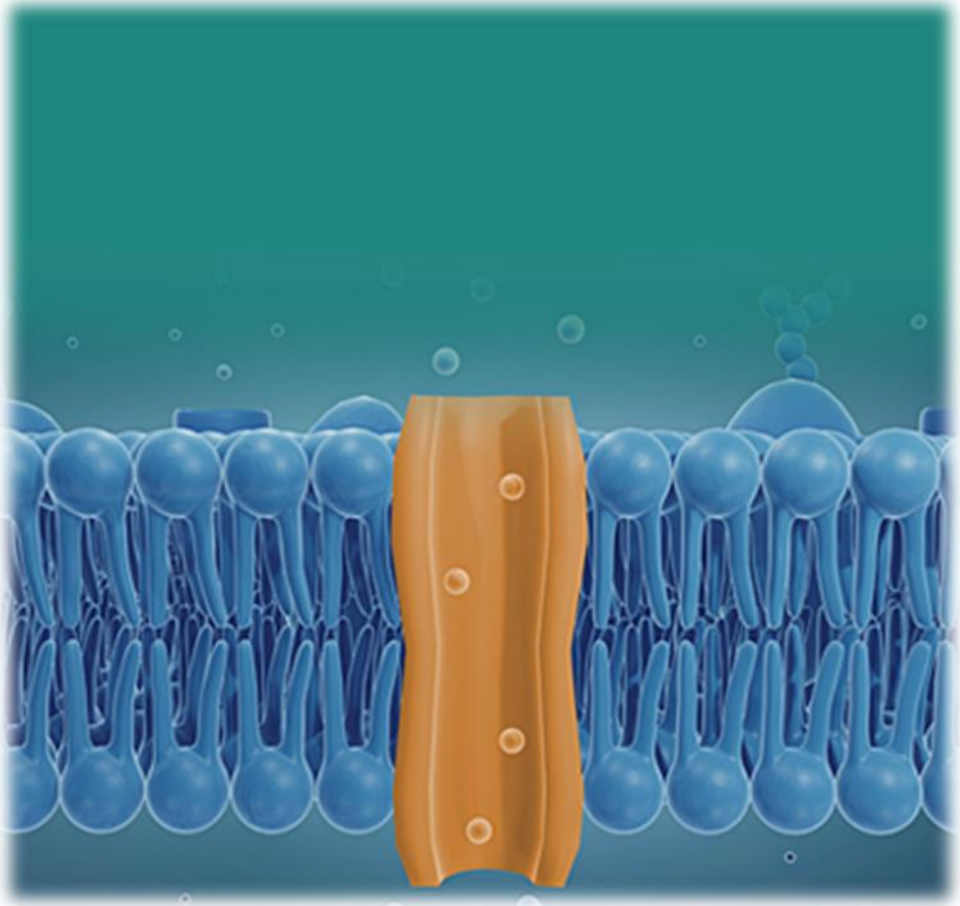

Click Channel Type to Access Validation Data:

$Ca_V1.2$ $\alpha1_C/\beta_{2a}/\alpha_2\delta_1$

$Ca_V2.2$ $\alpha1_B/\beta_3/\alpha_2\delta_1$

$Ca_V3.2$

Voltage-Gated Ca^{2+} Channels Introduction

BACK

The voltage-gated Ca^{2+} channel family consist of ten channels that have been characterized in mammals. Calcium channels are key transducers of membrane potential changes into local intracellular Ca^{2+} influx that initiates many different physiological events. Ca^{2+} influx regulates intracellular processes including secretion, neurotransmission, muscle contraction, and gene expression in many different cell types [1-2].

Ca^{2+} channels have been well-characterized and are complex proteins comprised of four to five distinct subunits [1,3-4]. The pore forming α_1 subunit is the largest subunit (190-250 kD). In addition to the pore, the α_1 subunit contains the voltage sensor and gating functionality, and the majority of binding sites for toxins, drugs and second messengers. Ca_{2+} channels also consist of an intracellular β subunit, a transmembrane, a α2δ subunit complex, and a transmembrane γ subunit [4].

Voltage-Gated Ca^{2+} Channel Classification and Nomenclature

BACK

Early studies of Ca^{2+} currents revealed diverse pharmacological and electrophysiological properties. Letter designations evolved for the different classes of Ca^{2+} currents [5-6], as well as low voltage activated (LVA) and high voltage activated (HVA) categories. L-type HVA Ca^{2+} currents require a depolarization above ~-40 mV for activation, are long-lasting (little inactivation), and are blocked by dihydropyridines, phenylalkylamines, and benzothiazepines [7-8]. L-type Ca^{2+} currents are the predominant Ca^{2+} channel in endocrine and muscle cells, where they initiate secretion and contraction. Other primarily neuronal HVA Ca^{2+} channel types that have been identified are N-type, P/Q-type, and R-type [7,9-10]. They are blocked by specific toxins from spider and snail venoms and relatively insensitive to L-type Ca^{2+} blockers [11]. T-type Ca^{2+} are LVA currents activated by depolarized voltages above about -60 mV, the currents produced inactivate, T- stands for transient currents [12-13]. They are resistant to both the L-type antagonists as well as the snake and spider toxins used to define HVA channels. Physiologically T-type channels are expressed in a wide variety excitable cells, where they are involved in controlling the patterns of repetitive firing, and in the kinetics of the action potential.

In 1994, a new nomenclature was adopted in which the α_1 pore forming subunits were referred to as α_{1S} for the HVA calcium channel in skeletal muscle, and α_{1A} through α_{1E} for the other HVA channels [14]. In 2000, a newer nomenclature was adopted similar to that adopted previously for potassium channels nomenclature [15-16]. The new nomenclature for voltage-gated Ca^{2+} channels is Ca_V for the permeating ion and voltage regulation. The numerical identifier corresponds to the Ca_V channel α_1 subunit gene 3 subfamilies (e.g. Ca_V1), followed by the temporal appearance in the literature of the α_1 subunit within that subfamily (e.g. $Ca_V1.1$). The α_1 subunit amino acid sequences are more than 70% identical within a subfamily, and less than 40% identical across the subfamilies.

Ca^{2+} Channel Regulation and Channelopathies

BACK

Ca^{2+} channels are regulated by G protein βγ subunits, phosphorylation by several protein kinases, calmodulin, Ca^{2+} binding proteins, and SNARE proteins, [2,17-21]. These are transient protein-protein interactions, stable interactions with members of the RGK-family of Ras-like GTP-binding proteins also occur that regulate Ca^{2+} channel localization and expression by binding to the intracellular β subunit [22].

Voltage-gated Ca^{2+} channel mutations cause many inherited channelopathies [23]. Hypokalemic periodic paralysis in skeletal muscle has been linked to $Ca_V1.1$ channel mutations [17]. Neuronal and cardiac $Ca_V1.2$ channels mutations that cause loss of voltage-dependent inactivation lead to cause Timothy Syndrome which includes cardiac arrhythmia, autism, and developmental abnormalities [24-26]. $Ca_V1.3$ loss of function mutants cause sinoatrial node dysfunction and deafness [29], gain of function of $Ca_V1.3$ is implicated in autism and severe neurodevelopmental disorders, as well as primary aldosteronism [30]. Gain of function in $Ca_V2.1$ channels has been implicated in causing migraine headaches, and other mutations of $Ca_V2.1$ cause spinocerebellar ataxia type 6 [31-33]. Congenital stationary night blindness has been linked to loss of function mutations of $Ca_V1.4$ channels [34-35]. Other calcium channelopathies include epileptic encephalopathies have been linked to $Ca_V2.3$ and childhood-onset cerebellar ataxia linked to $Ca_V3.1$ [36-37]

References

1) Catterall WA. (2011) Voltage-gated calcium channels. Cold Spring Harb Perspect Biol, 3 (8): a003947. [PMID:21746798]

2) Zamponi GW, Striessnig J, Koschak A, Dolphin AC. (2015) The Physiology, Pathology, and Pharmacology of Voltage-Gated Calcium Channels and Their Future Therapeutic Potential. Pharmacol Rev, 67 (4): 821-70. [PMID:26362469]

3) Striessnig J. (1999) Pharmacology, structure and function of cardiac L-type Ca(2+) channels. Cell Physiol Biochem, 9 (4-5): 242-69. [PMID:10575201]

4) Takahashi M, Seagar MJ, Jones JF, Reber BF, Catterall WA. (1987) Subunit structure of dihydropyridine-sensitive calcium channels from skeletal muscle. Proc Natl Acad Sci U S A, 84 (15): 5478-5482. [PMID:2440051]

5) Snutch TP, Leonard JP, Gilbert MM, Lester HA, Davidson N. (1990) Rat brain expresses a heterogeneous family of calcium channels. Proc Natl Acad Sci USA, 87 (9): 3391-3395. [PMID:1692134]

6) Tsien RW, Lipscombe D, Madison D, Bley K, Fox A. (1995) Reflections on Ca(2+)-channel diversity, 1988-1994. Trends Neurosci, 18 (2): 52-4. [PMID:7537405]

7) Nowycky MC, Fox AP, Tsien RW. (1985) Three types of neuronal calcium channel with different calcium agonist sensitivity. Nature, 316 (6027): 440-3. [PMID:2410796]

8) Reuter H. (1979) Properties of two inward membrane currents in the heart. Annu Rev Physiol, 41: 413-24. [PMID:373598]

9) Llinás R, Sugimori M, Hillman DE, Cherksey B. (1992) Distribution and functional significance of the P-type, voltage-dependent Ca2+ channels in the mammalian central nervous system. Trends Neurosci, 15 (9): 351-5. [PMID:1382335]

10) Randall A, Tsien RW. (1995) Pharmacological dissection of multiple types of Ca2+ channel currents in rat cerebellar granule neurons. J Neurosci, 15 (4): 2995-3012. [PMID:7722641]

11) Olivera BM, Miljanich GP, Ramachandran J, Adams ME. (1994) Calcium channel diversity and neurotransmitter release: the omega-conotoxins and omega-agatoxins. Annu Rev Biochem, 63: 823-67. [PMID:7979255]

12) Carbone E, Lux HD. (1984) A low voltage-activated, fully inactivating Ca channel in vertebrate sensory neurones. Nature, 310 (5977): 501-2. [PMID:6087159]

13) Perez-Reyes E, Cribbs LL, Daud A, Lacerda AE, Barclay J, Williamson MP, Fox M, Rees M, Lee JH. (1998) Molecular characterization of a neuronal low-voltage-activated T-type calcium channel. Nature, 391 (6670): 896-900. [PMID:9495342]

BACK

References

14) Birnbaumer L, Campbell KP, Catterall WA, Harpold MM, Hofmann F, Horne WA, Mori Y, Schwartz A, Snutch TP, Tanabe T et al.. (1994) The naming of voltage-gated calcium channels. Neuron, 13 (3): 505-6. [PMID:7917287]

15) Ertel EA, Campbell KP, Harpold MM, Hofmann F, Mori Y, Perez-Reyes E, Schwartz A, Snutch TP, Tanabe T, Birnbaumer L, Tsien RW, Catterall WA. (2000) Nomenclature of voltage-gated calcium channels. Neuron, 25 (3): 533-5. [PMID:10774722]

16) Chandy KG, Gutman GA. (1993) Nomenclature for mammalian potassium channel genes. Trends Pharmacol Sci, 14 (12): 434. [PMID:8122319]

17) Catterall WA. (2000) Structure and regulation of voltage-gated Ca2+ channels. Annu Rev Cell Dev Biol, 16: 521-55. [PMID:11031246]

18) Catterall WA. (2015) Regulation of Cardiac Calcium Channels in the Fight-or-Flight Response. Curr Mol Pharmacol, 8 (1): 12-21. [PMID:25966697]

19) Hofmann F, Lacinová L, Klugbauer N. (1999) Voltage-dependent calcium channels: from structure to function. Rev Physiol Biochem Pharmacol, 139: 33-87. [PMID:10453692]

20) Nanou E, Catterall WA. (2018) Calcium Channels, Synaptic Plasticity, and Neuropsychiatric Disease. Neuron, 98 (3): 466-481. [PMID:29723500]

21) Reuter H. (1983) Calcium channel modulation by neurotransmitters, enzymes and drugs. Nature, 301 (5901): 569-74. [PMID:6131381]

22) Buraei Z, Yang J. (2015) Inhibition of Voltage-Gated Calcium Channels by RGK Proteins. Curr Mol Pharmacol, 8 (2): 180-7. [PMID:25966691]

23) Nanou E, Catterall WA. (2018) Calcium Channels, Synaptic Plasticity, and Neuropsychiatric Disease. Neuron, 98 (3): 466-481. [PMID:29723500]

24) Marcantoni A, Calorio C, Hidisoglu E, Chiantia G, Carbone E. (2020) Cav1.2 channelopathies causing autism: new hallmarks on Timothy syndrome. Pflugers Arch, 472 (7): 775-789. [PMID:32621084]

25) Splawski I, Timothy KW, Decher N, Kumar P, Sachse FB, Beggs AH, Sanguinetti MC, Keating MT. (2005) Severe arrhythmia disorder caused by cardiac L-type calcium channel mutations. Proc Natl Acad Sci USA, 102 (23): 8089-8096; discussion 8086-8088. [PMID:15863612]

26) Splawski I, Timothy KW, Sharpe LM, Decher N, Kumar P, Bloise R, Napolitano C, Schwartz PJ, Joseph RM, Condouris K et al.. (2004) Ca(V)1.2 calcium channel dysfunction causes a multisystem disorder including arrhythmia and autism. Cell, 119 (1): 19-31. [PMID:15454078]

27) Flucher BE. (2020) Skeletal muscle CaV1.1 channelopathies. Pflugers Arch, 472 (7): 739-754. [PMID:32222817]

BACK

References

28) Venance SL, Cannon SC, Fialho D, Fontaine B, Hanna MG, Ptacek LJ, Tristani-Firouzi M, Tawil R, Griggs RC, CINCH investigators. (2006) The primary periodic paralyses: diagnosis, pathogenesis and treatment. Brain, 129 (Pt 1): 8-17. [PMID:16195244]

29) Baig SM, Koschak A, Lieb A, Gebhart M, Dafinger C, Nürnberg G, Ali A, Ahmad I, Sinnegger-Brauns MJ, Brandt N et al.. (2011) Loss of Ca(v)1.3 (CACNA1D) function in a human channelopathy with bradycardia and congenital deafness. Nat Neurosci, 14 (1): 77-84. [PMID:21131953]

30) Ortner NJ, Kaserer T, Copeland JN, Striessnig J. (2020) De novo CACNA1D Ca2+ channelopathies: clinical phenotypes and molecular mechanism. Pflugers Arch, 472 (7): 755-773. [PMID:32583268]

31) Ophoff RA, Terwindt GM, Vergouwe MN, van Eijk R, Oefner PJ, Hoffman SM, Lamerdin JE, Mohrenweiser HW, Bulman DE, Ferrari M et al.. (1996) Familial hemiplegic migraine and episodic ataxia type-2 are caused by mutations in the Ca2+ channel gene CACNL1A4. Cell, 87 (3): 543-52. [PMID:8898206]

32) Zhuchenko O, Bailey J, Bonnen P, Ashizawa T, Stockton DW, Amos C, Dobyns WB, Subramony SH, Zoghbi HY, Lee CC. (1997) Autosomal dominant cerebellar ataxia (SCA6) associated with small polyglutamine expansions in the alpha 1A-voltage-dependent calcium channel. Nat Genet, 15 (1): 62-9. [PMID:8988170]

33) Pietrobon D, Striessnig J. (2003) Neurobiology of migraine. Nat Rev Neurosci, 4 (5): 386-98. [PMID:12728266]

34) Bech-Hansen NT, Naylor MJ, Maybaum TA, Pearce WG, Koop B, Fishman GA, Mets M, Musarella MA, Boycott KM. (1998) Loss-of-function mutations in a calcium-channel alpha1-subunit gene in Xp11.23 cause incomplete X-linked congenital stationary night blindness. Nat Genet, 19 (3): 264-7. [PMID:9662400]

35) Strom TM, Nyakatura G, Apfelstedt-Sylla E, Hellebrand H, Lorenz B, Weber BH, Wutz K, Gutwillinger N, Rüther K, Drescher B et al.. (1998) An L-type calcium-channel gene mutated in incomplete X-linked congenital stationary night blindness. Nat Genet, 19 (3): 260-3. [PMID:9662399]

36) Helbig KL, Lauerer RJ, Bahr JC, Souza IA, Myers CT, Uysal B, Schwarz N, Gandini MA, Huang S, Keren B et al.. (2018) De Novo Pathogenic Variants in CACNA1E Cause Developmental and Epileptic Encephalopathy with Contractures, Macrocephaly, and Dyskinesias. Am J Hum Genet, 103 (5): 666-678. [PMID:30343943]

37) Chemin J, Siquier-Pernet K, Nicouleau M, Barcia G, Ahmad A, Medina-Cano D, Hanein S, Altin N, Hubert L, Bole-Feysot C et al.. (2018) De novo mutation screening in childhood-onset cerebellar atrophy identifies gain-of-function mutations in the CACNA1G calcium channel gene. Brain, 141 (7): 1998-2013. [PMID:29878067]

BACK

$Ca_V1.2\ \alpha_{1C}/\beta_{2a}/\alpha_2\delta_1$ (CYL3051)

BACK

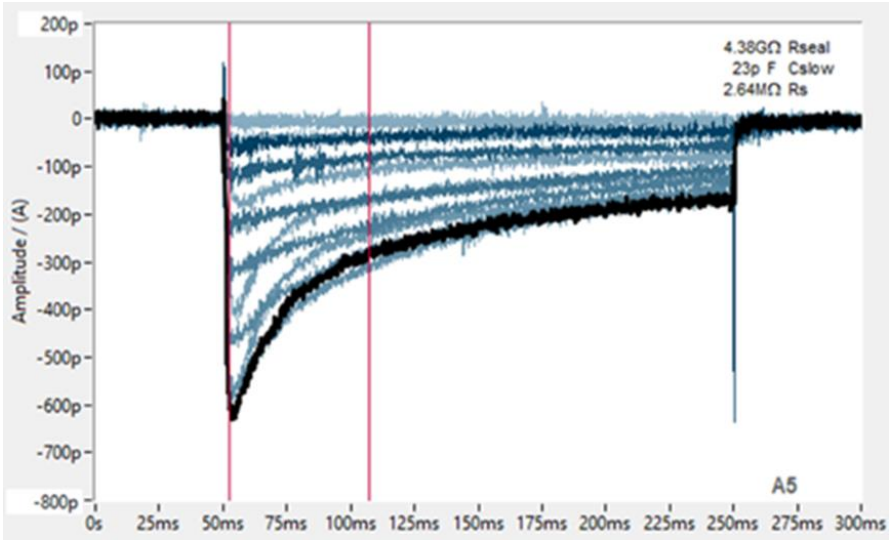

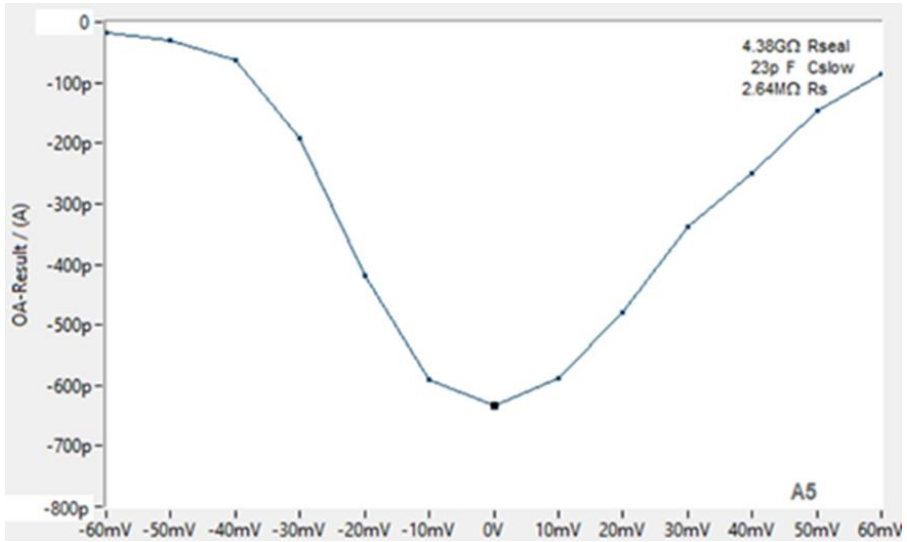

Cav1.2 $\alpha_{1C}/\beta_{2a}/\alpha_2\delta_1$ currents expressed in HEK-293 cells measured in the whole cell mode. **Left Panel:** Raw ionic current traces for the current-voltage (I/V) plot shown in the **right panel.** Currents were elicited by stepping from a holding potential -100 mV to -60 mV then increasing in 10 mV increments to +60 mV.. (SyncroPatch 384i Data)

$Ca_V1.2$

BACK

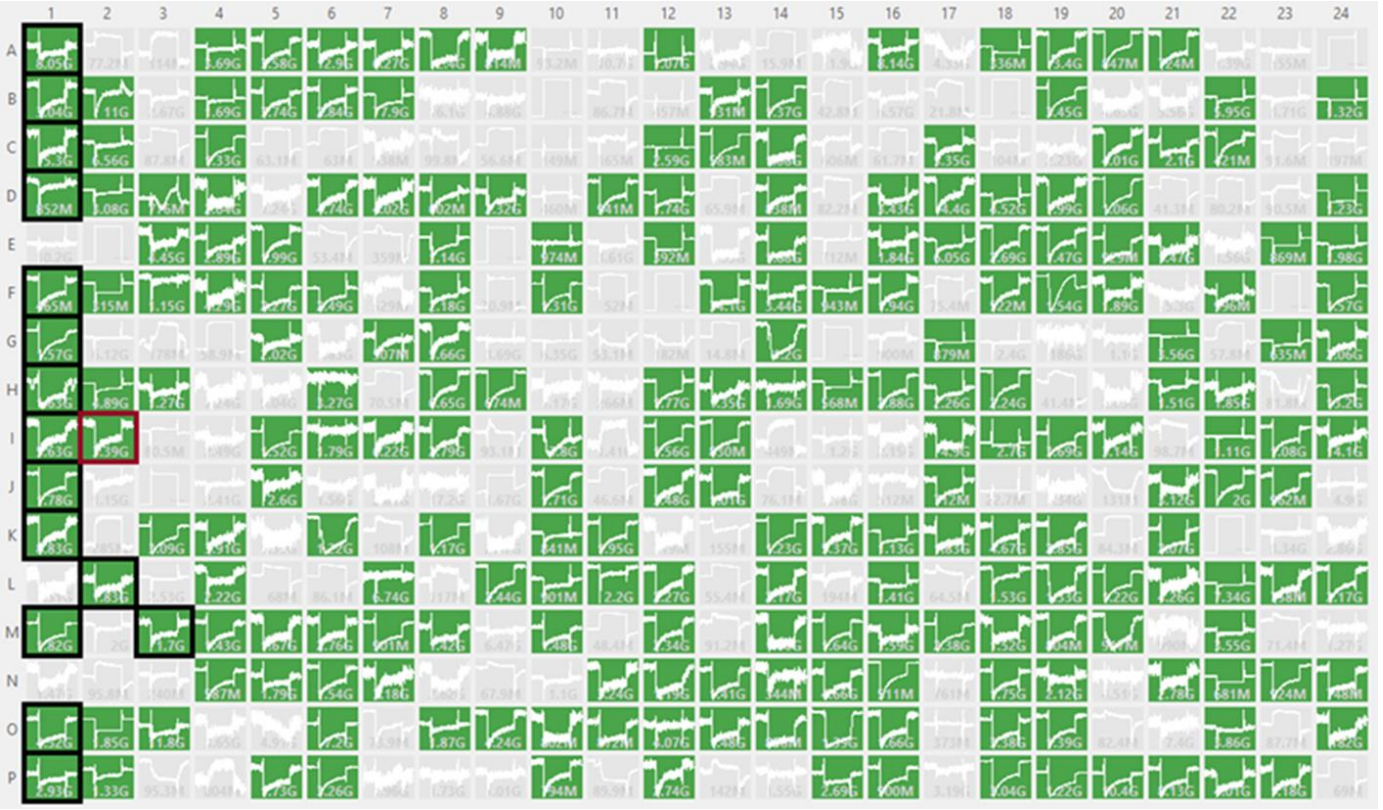

Cav1.2 currents expressed in HEK-293 cells. Success rates of 59.1% was achieved prior to the addition of nitrendipine (wells with current smaller than -75 pA and seals below 300 MΩ are filtered out). (SyncroPatch 384i Data)

$Ca_V1.2$

BACK

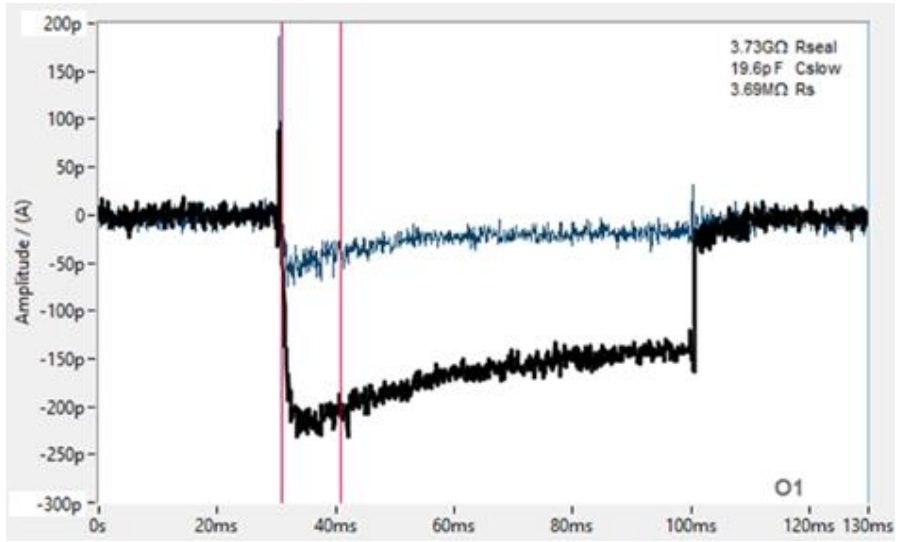

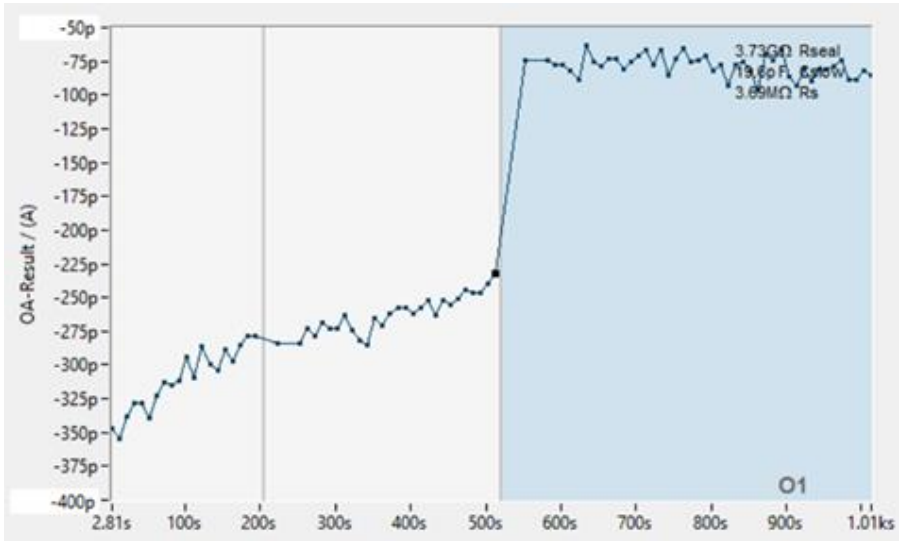

Pharmacological blockade of Cav1.2 currents by nitrendipine. Left Panel: Raw ionic current traces prior to (black trace) and after the addition of 200 µM nitrendipine (blue trace). Currents are elicited by a step from the holding potential of -100 mV to -10 mV. **Right Panel:** Current-Time (I/t) plot of currents prior to the addition of 200 µM nitrendipine, and then blockade by nitrendipine added at the start of the blue shaded portion of the I/t plot. (SyncroPatch 384i Data)

$Ca_V1.2$

BACK

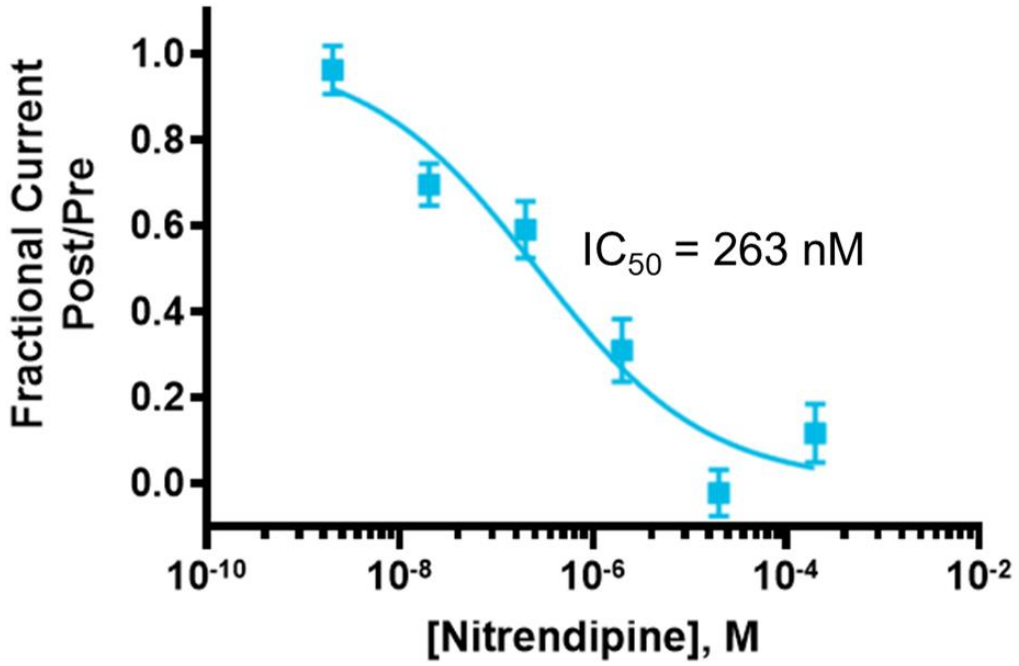

Dose response curve for the blockade of Cav1.2 by nitrendipine. In this experiment we obtained an IC_{50} of 263 nM. (SyncroPatch 384i Data)

$Ca_V2.2\ \alpha_{1B}/\beta_3/\alpha_2\delta_1$ (CYL3054)

BACK

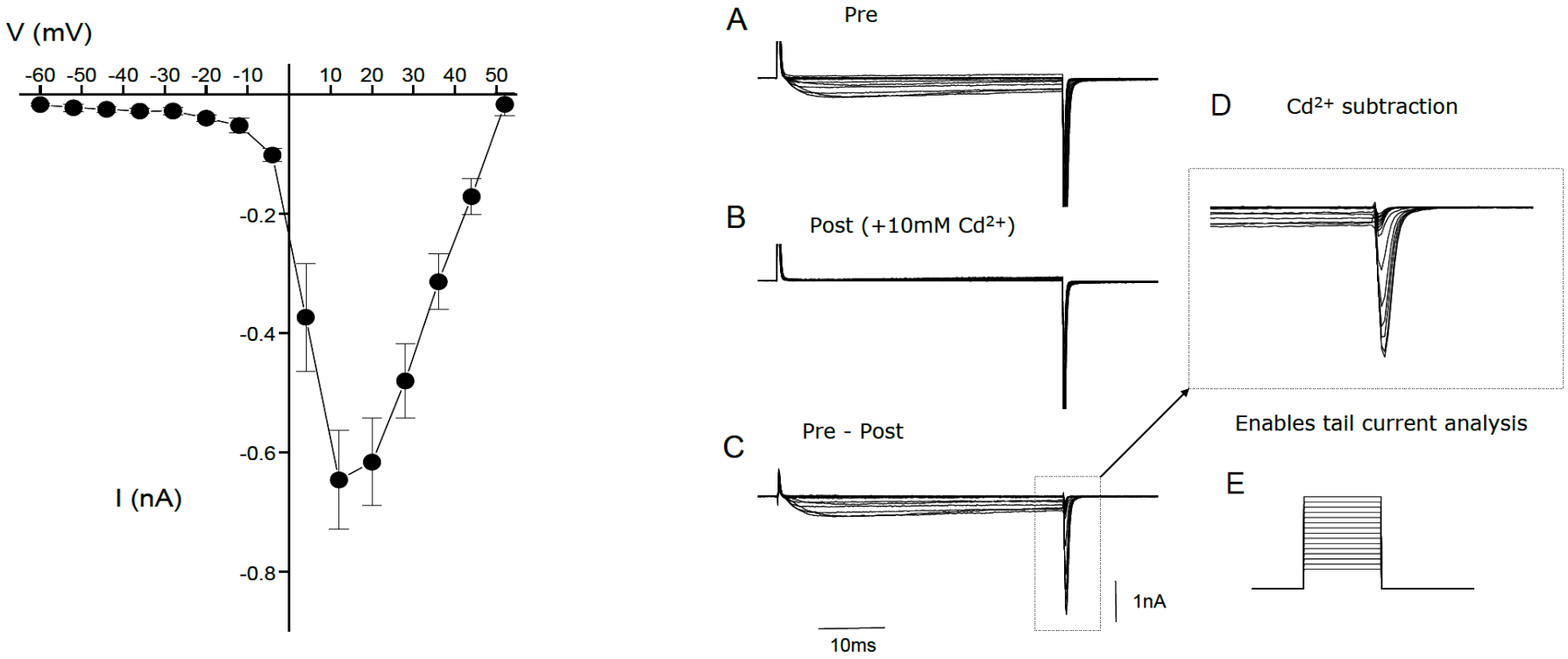

hCav2.2 $\alpha_{1B}/\beta_3/\alpha_2\delta_1$ Current-Voltage (I/V) Relationship and Voltage Dependence of Activation: **Left:** The voltage was stepped from a holding potential of -90 mV to voltages of -60 mV to +52 mV for 40 ms every 500 ms. Peak currents during the 40 ms step are plotted against the relevant test step. Currents were recorded using 10 mM Ba2+ external solution (n=15 cells). **Right:** Using the voltage protocol described above (Figure 1), and subtracting the currents from the corresponding currents evoked in the presence of 10 µM Cd2+, it was possible to measure hCav2.2 tail current amplitudes free from contaminating currents and capacity currents (Figure 2). Cd2+ Subtraction: Example currents elicited by 40 ms steps to various test potentials. A. Currents obtained pre-Cd2+ addition, B. Currents obtained after addition of 10 mM Cd2+, C. Current values obtained after Cd2+ subtraction, D. Tail currents, E. Voltage protocol. (IonWorks HT Data)

$Ca_V2.2$

BACK

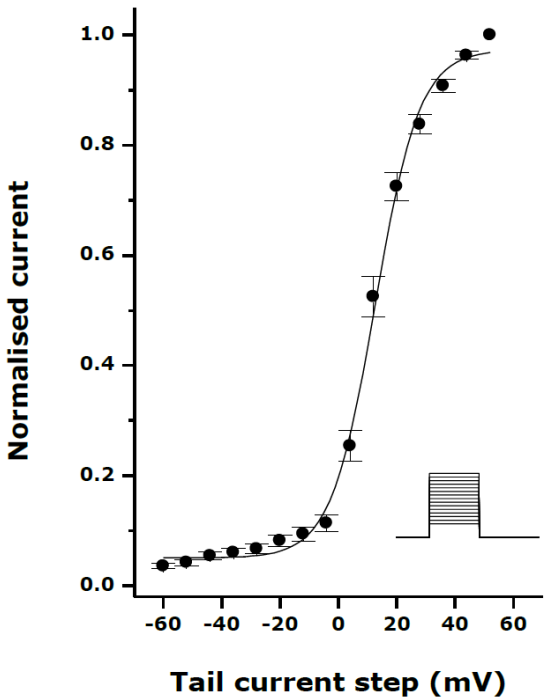

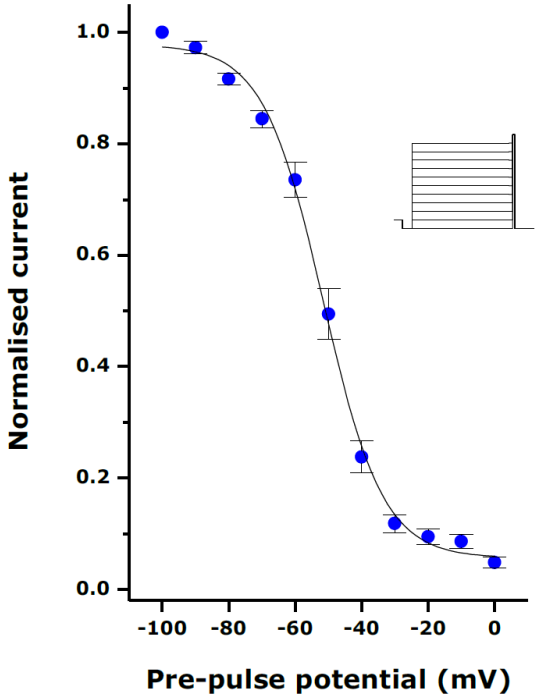

hCAV2.2 Current Activation and Inactivation: **Left:** The instantaneous currents, evoked on repolarization to the holding potential (-90 mV) following the 40 ms pre-pulse steps were measured. Currents were normalized to the current evoked with a pre-pulse potential of +52 mV and plotted against pre-pulse potential voltages. A Boltzmann fit of the data yielded a V½ of activation of +13 ± 1 mV (mean ± SEM). **Inset:** Voltage protocol. **Right:** Currents evoked by the test pulse were normalized to the current evoked by a test pulse following a pre-pulse of at -100 mV and plotted against voltage. A Boltzmann fit of the data yielded a V½ of inactivation of -51 ± 2 mV and a slope (k) of 8.5 ± 0.7 mV (n=9), mean ± SEM. **Inset:** Voltage protocol. (IonWorks HT Data)

$Ca_V2.2$

BACK

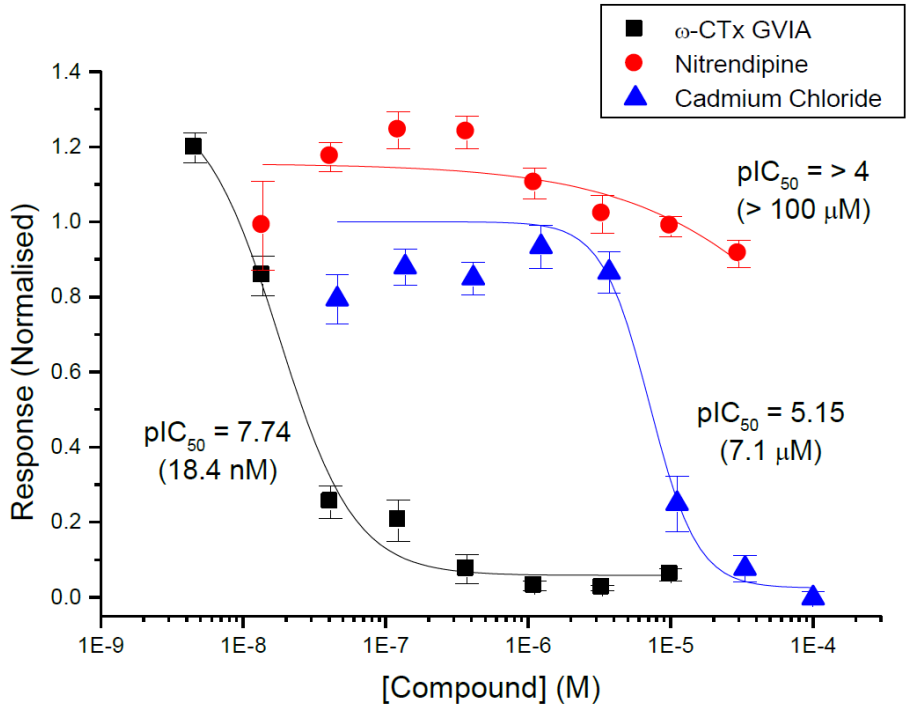

$hCa_V2.2$ Pharmacology: The affinity of the highly selective N-type calcium blocking agent ω-conotoxin GVIA (ω-CTx GVIA - a peptide toxin from the snail Conus geographus), was compared to $CdCl_2$ and the dihydropyridine L-type calcium-channel blocker nitrendipine. Confirming the selective expression of hCav2.2 currents, nitrendipine was essentially without effect whereas the snail toxin potently blocked the current (IC_{50} = 18.4 nM). Responses are normalised to the currents obtained without the addition of blocker (IonWorks HT Data)

$Ca_V3.2$ (CYL3075)

BACK

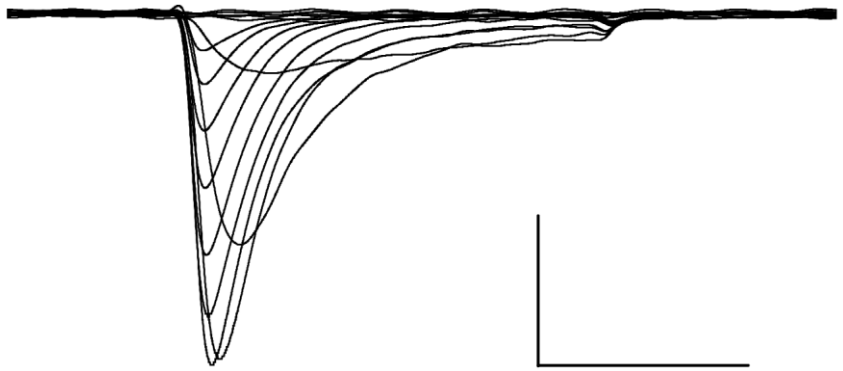

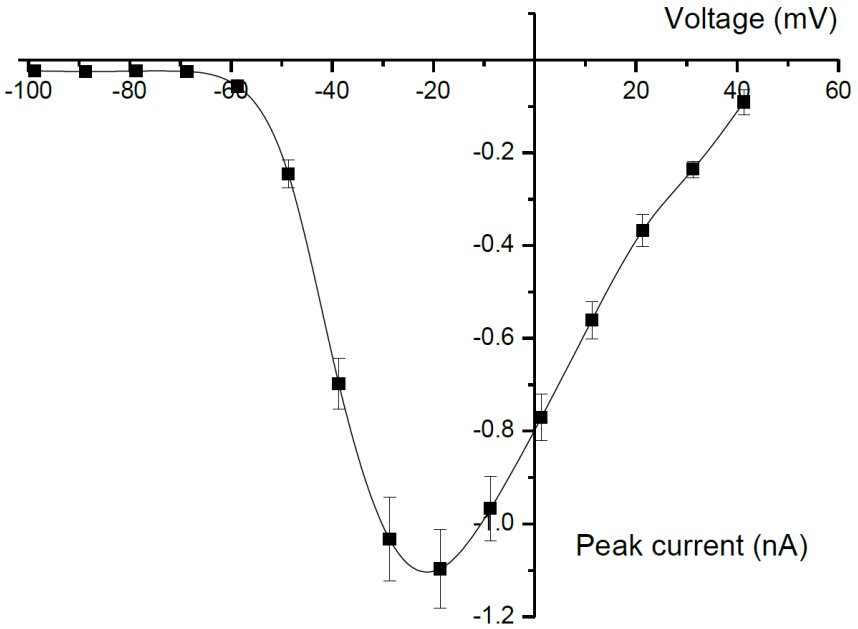

hCa$_V$3.2 Raw Data Currents and Current-Voltage (I/V) Relationship: **Left:** Ca$_V$3.2 currents were evoked by 100 ms depolarizing voltage pulses stepped in 10 mV increments from -90 mV to +50 mV from a holding potential of –90 mV once every 5 seconds. Scale bars represent 50 ms and 500 pA. **Right:** Current-voltage relationship of Cav3.2. The mean peak currents evoked during the 100 ms voltage step are plotted against the step potential in millivolts (n= 4) (Manual Patch Clamp Data)

$Ca_V3.2$

BACK

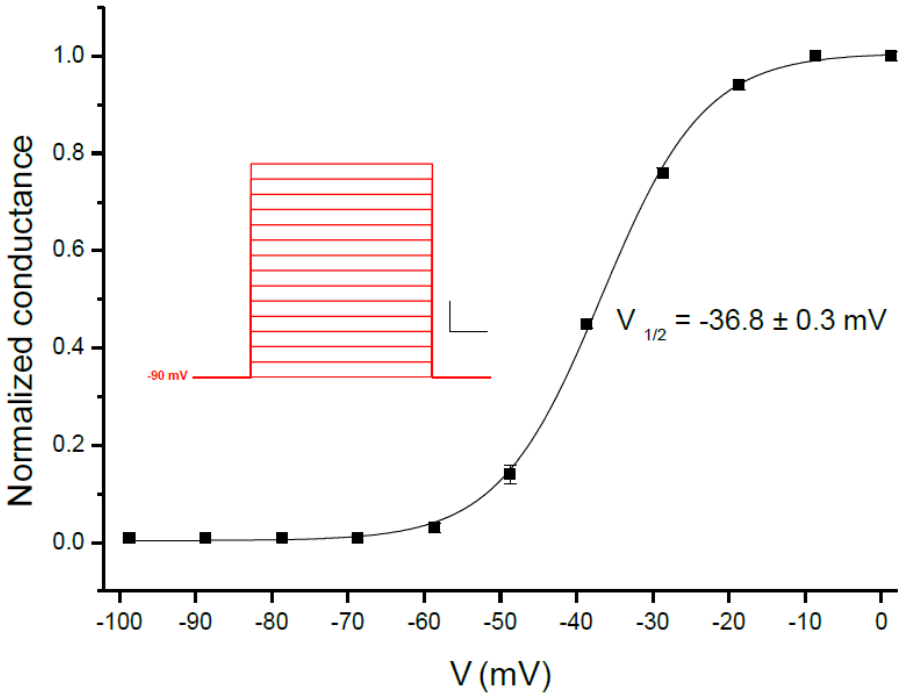

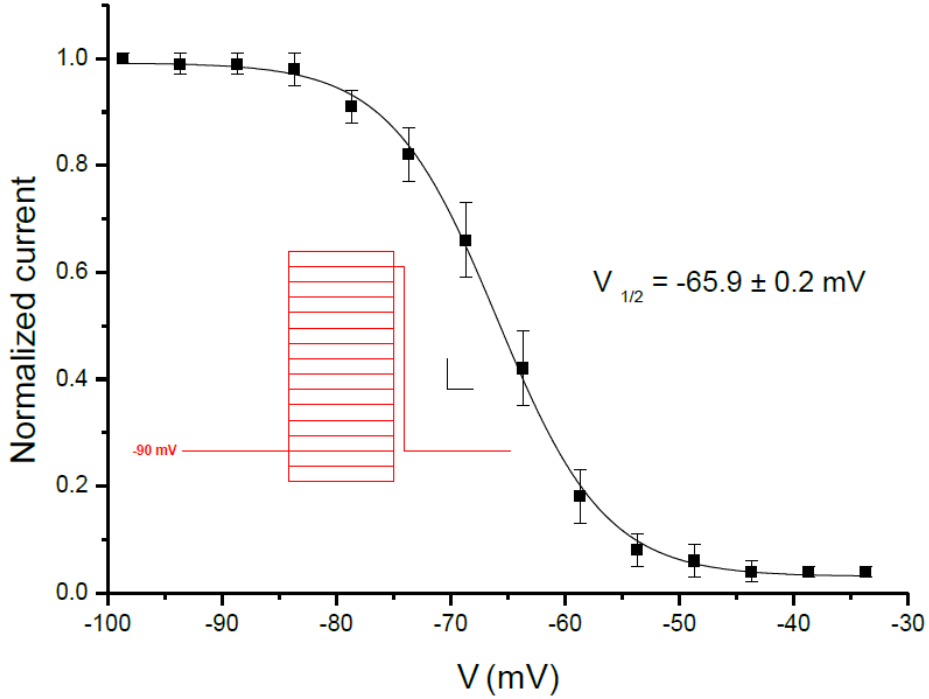

hCa$_V$3.2 Voltage Dependence of Activation and Inactivation: **Left:** Conductance was normalized to conductance at 0 mV and plotted against membrane voltage. Data was described with a Boltzmann equation with a V½ of activation of -36.8 ± 0.3 mV and slope (k) of 6.8 ± 0.3 mV. Values represent means ± SEM (n = 4). The voltage protocol used is shown (inset). Scale bars represent 20 ms and 20 mV. **Right:** The voltage-Dependence of inactivation. The voltage was first stepped to various voltages from -100 mV to -25 mV in 5 mV increments for 1s from a holding potential of -90 mV. After each pre-pulse voltage step there was a subsequent step to -30 mV (to measure channel availability) followed by a step to -90 mV. Peak hCav3.2 currents at -30 mV were normalized to maximal current, evoked with a pre-pulse potential of -90 mV, and plotted against the relevant pre-pulse potential voltage (Figure 3). This could be described by a Boltzmann equation giving an estimated V½ of inactivation was -65.9 ± 0.2 mV and a slope (k) of 4.7 ± 0.2 mV (n = 4). The voltage protocol used is shown (inset). Scale bars represent 250 ms and 10 mV. (Manual Patch Clamp Data)

$Ca_V3.2$

BACK

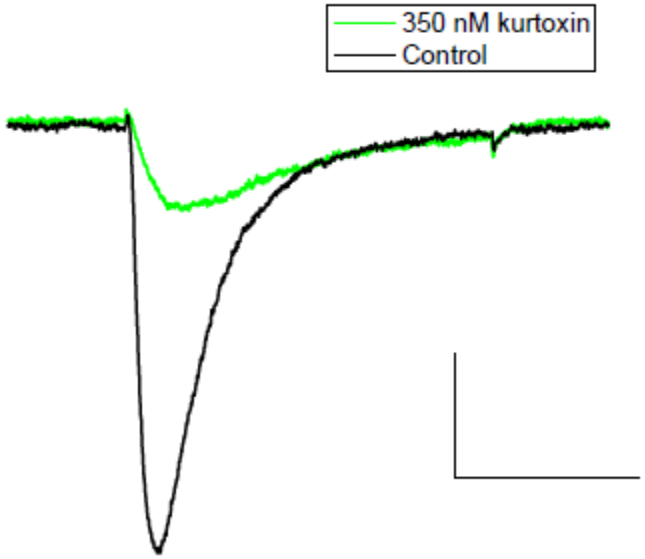

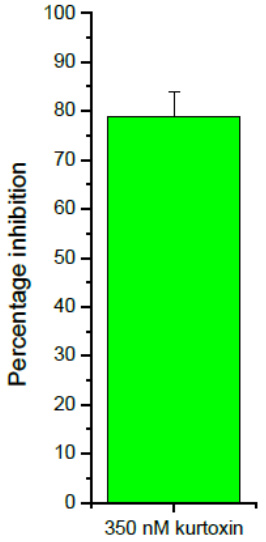

Blockade of $hCa_V3.2$ currents by Kurtoxin: **Left:** Typical traces showing the effect of 350 nM kurtoxin. Calcium currents are shown before (black trace) and in the presence of kurtoxin (green trace). The cells were held at a holding potential of –90 mV and then stepped to -30 mV for 100 ms. Scale bars represent 100 ms and 500 pA. **Right:** Mean inhibition by 350 nM kurtoxin. Cells were stepped to a potential of –30 from a holding potential of -100 mV. The amplitude of the current is expressed as relative current compared to the control response (n = 3) (Manual Patch Clamp Data)

$Ca_V3.2$

BACK

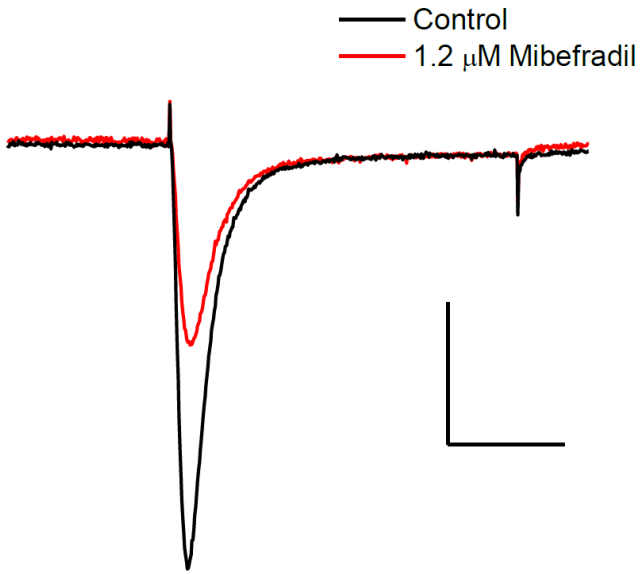

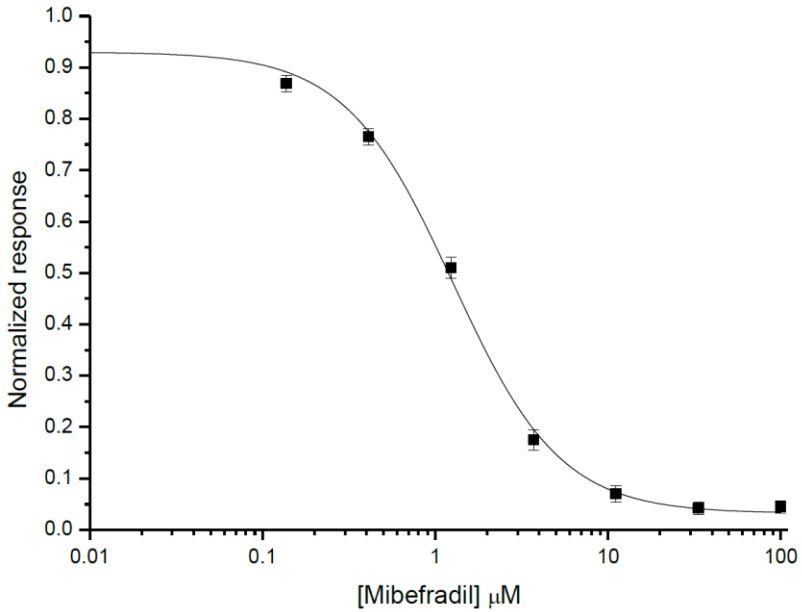

Blockade of $hCa_V3.2$ Currents by Mibefradil: **Left:** Typical traces showing the effect of 1.2 μM mibefradil. Calcium currents are shown before (black trace) and in the presence of mibefradil (red trace). The cells were held at a holding potential of –100 mV and then stepped to -30 mV for 300 ms. Scale bars represent 100 ms and 500 pA. **Right:** Dose-response curve of mibefradil on hCav3.2. Cells were stepped to a potential of –30 from a holding potential of -100 mV. The amplitude of the current is expressed as relative current compared to the control response. These values were plotted against concentration to obtain the dose-response curve. This could be described by a Hill equation with an estimated IC50 value of 1.3 ± 0.1 μM (n = 10 – 39) (IonWorks HT Data)

$Ca_V3.2$

BACK

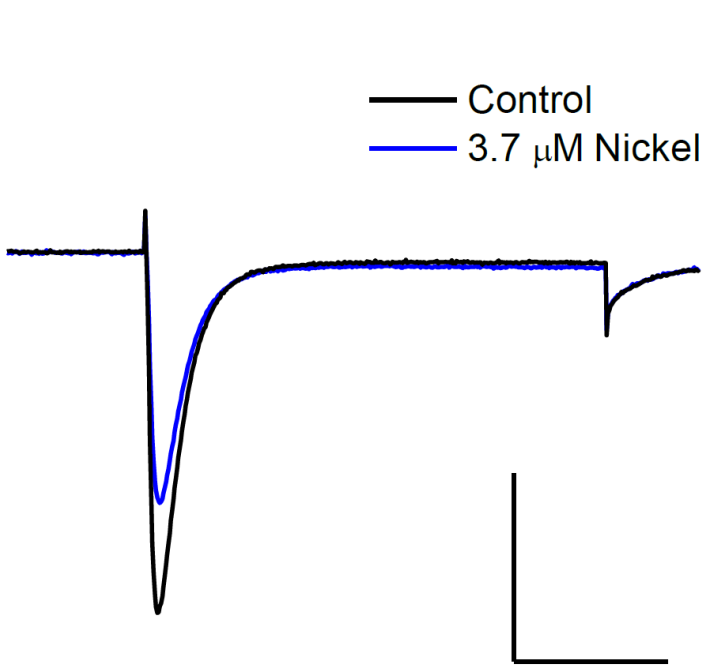

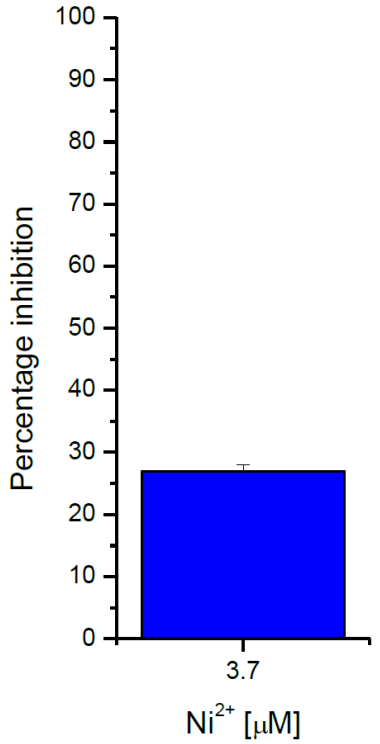

Effect of Nickel on $hCa_V3.2$ Currents: **Left:** Typical traces showing the effect of 3.7 μM nickel. Calcium currents are shown before (black trace) and in the presence of nickel (blue trace). The cells were held at a holding potential of –100 mV and then stepped to -30 mV for 300 ms. Scale bars represent 100 ms and 500 pA. **Right:** Mean inhibition by 3.7 μM nickel. Cells were stepped to a potential of –30 from a holding potential of -100 mV. The amplitude of the current is expressed as relative current compared to the control response (n = 39) (IonWorks Quattro Data)

$Ca_V3.2$

BACK

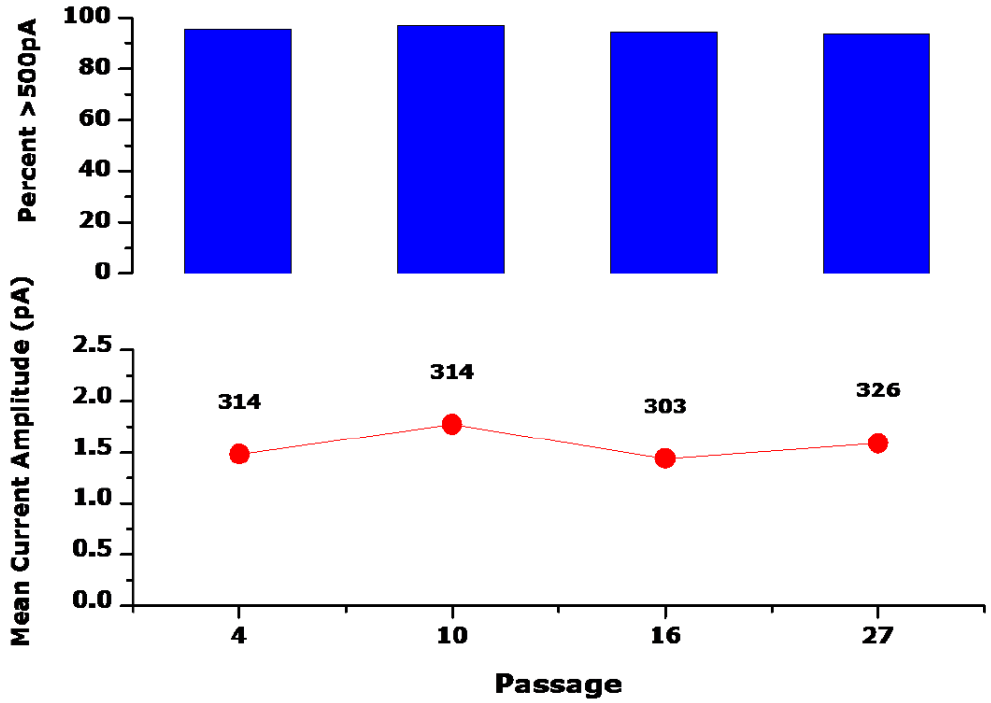

$hCa_V3.2$ Stability of Expression Over Passage: The upper panel shows the percentage of cells expressing a mean peak tail current >500 pA at -30 mV at cell passages 4, 10, 16 and 27. The lower panel shows the mean current amplitude (mean ± SEM, red circles) and the number of these cells (numbers above red circles) (IonWorks HT Data).